Hindawi Publishing Corporation
Advances in Condensed Matter Physics
Volume 2014, Article ID 957067, 7 pages
http://dx.doi.org/10.1155/2014/957067

Research Article

Numerical Analysis of Oxygen Adsorption on SnO_2 Surface Using Slab Geometry

Weronika Izydorczyk

Institute of Electronics, Faculty of Automatic Control, Electronics and Computer Science, Silesian University of Technology, Akademicka 16, 44-100 Gliwice, Poland

Correspondence should be addressed to Weronika Izydorczyk; weronika.izydorczyk@polsl.pl

Received 31 May 2013; Accepted 21 October 2013; Published 16 January 2014

Academic Editor: Jörg Fink

Oxidation of thin film SnO_2 layer was simulated. In particular, the evolution of depletion layer was investigated by solving Poisson-Boltzmann equation for SnO_2 slab geometry grains. On this basis, the surface energy barrier dependence on layer thickness (30–500 nm) was obtained. The effect of the donor mobility (oxygen vacancies in the bulk) and degree of donor ionization on electric potential inside layer with different thicknesses was discussed. Furthermore, the dependence of per-square conductance on temperature (from 400 K to 700 K) has been computed. It was assumed that the bulk oxygen vacancies (donors) are singly or doubly ionized and mobile. The temperature variations in the carrier mobility were also taken into account.

1. Introduction

Tin dioxide (SnO_2) is a semiconductor oxide with a wide range of applications. The material is being used as a photocatalyst and a gas sensor and in optical devices [1–3]. In all these applications, the surface-related phenomena play a major role and become particularly important for nanomaterials, in which surface-to-volume ratio is much higher [4–6]. Precise numerical model of electrical properties of near-surface layer of SnO_2 grains is fundamental for improving sensitivity and selectivity of SnO_2 based gas sensors [6]. Shape and size of SnO_2 nanograins are considered the most important factors for film conductance. It is caused by chemical reactions which take place on the surface of SnO_2 grains. In particular, oxygen adsorption on the surface of SnO_2 (ZnO and TiO_2) decreases concentration of electrons in the near-surface layer. Depleted region is formed and conductivity of the layer is decreased. At the same time range of working temperatures of the film is raised from 420 to 720 K. Despite much experimental and theoretical research [7–19], the role played by adsorbed oxygen in surface and volume phenomena (surface coverage by oxygen ions, band bending, and distribution of mobile donors) occurring in nanolayers of SnO_2 and the influence of these phenomena on conductivity have not yet been explained. Reversible changes in the conductivity of SnO_2 layer have been reported, caused by a change in partial pressure of oxygen for sensor work temperature exceeding 500 K. The observed conductivity changes fulfil the exponential relation $G \sim [P_{O_2}]^{\alpha}$, where α index assumes values from -0.25 to -0.5 or $\alpha = -1/6$ for temperatures above 1000 K [12]. Band bending caused by oxygen adsorption was reported by Mizsei and Lantto [13] and Semancik and Cox [14]. Also, X-ray photoelectron spectroscopy (XPS) was used to demonstrate band bending of 0.2 eV as a result of the interaction between oxygen and nanocrystalline layers of SnO_2 [15]. Furthermore, a theoretical analysis of oxygen adsorption on the stoichiometric surface and in the case when surface oxygen vacancies are present was carried out [13, 14]. Rantala and Lantto [18] calculated the height of the surface energy barrier (below 0.7 eV) for totally depleted grains of various diameters. Three grain geometries were discussed (flat, cylindrical, and spherical). In the calculations, it was assumed that donors are mobile and single or double ionized. As a result of the calculations, it was proved that thin tin dioxide layers placed in synthetic air can be totally depleted in terms of charge carriers. The thickness of these layers cannot exceed 0.25 μm and 1 μm (at $T = 573$ K) in the case of,

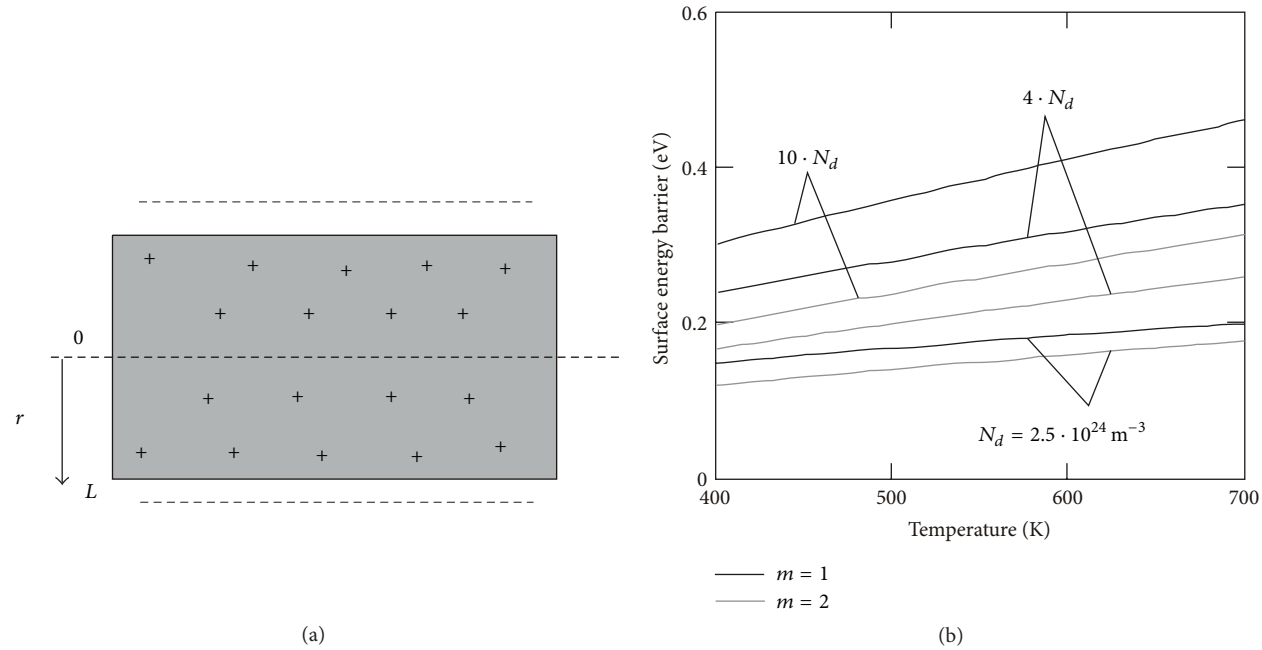

Figure 1: (a) The grain with slab geometry $r = 0$ at the grain center, $2 \times L$—slab thickness. (b) Full depletion layer. Surface energy barriers versus temperature, for different donor concentrations ($L = 15$ nm, $N_d = 2.5 \times 10^{24}\ \mathrm{m}^{-3}$, and $m = 1$ or 2).

respectively, mobile and single- and double-ionized donors. Thus, modeling sensor structures based on SnO_2 nanolayers requires allowing for the size and shape of grains, which determine, among others, the conductivity of those layers.

In the case of modeling electron properties of thin SnO_2 layers whose thickness is below 500 nm, one should additionally include the phenomenon of moving oxygen vacancies through the volume (the so-called mobile donors), which influence the distribution of potential within the layer.

The purpose of this work was a rigorous theoretical analysis of the influence of surface oxidation on the conductance of SnO_2 nanofilms. Influence on SnO_2 layers electrical properties of the assumption that oxygen vacancies are mobile was studied. From the one-dimensional analytical solution of the Poisson-Boltzmann equation in the case of finite grains with slab geometry, the in-depth profiles of the potential $V(r)$ were obtained for full depleted layers (following [18]). The SnO_2layer thickness was in the range from 30 nm to 500 nm. Then, the surface energy barrier dependence on temperature (from 400 K to 700 K) was determined. These magnitudes were calculated for different bulk doping, assuming that the bulk oxygen vacancies (donors) are singly or doubly ionized and mobile. These magnitudes were used as input data for computer simulations based on the rate equations proposed by Rantala et al. [4] for the electron transfer between the oxygen surface species and the bulk conduction band to calculate the total coverage by oxygen species and coverages by various oxygen ions. Subsequently, the in-depth profiles of carrier concentrations, distribution of donors, and per-square conductance dependence on temperature were obtained. Furthermore, the influence of partial oxygen pressure on the SnO_2 nanofilm conductance was studied.

2. Analytical Procedure

The in-depth potential profiles in the depletion region induced by gas adsorption and surface energy barrier heights were computed for one-dimensional SnO_2 grains with slab geometry (i.e., layer thickness $2 \times L$ is much lower than other dimensions; see Figure 1(a)) and n-type doping (donor concentration N_d) [20]. The electric potential $\phi(r)$ was obtained by solving the Poisson-Boltzmann equation [18]:

$$\frac{d^2\phi(r)}{dr^2} = -\frac{emN_{d0}}{\varepsilon\varepsilon_0}\exp\left(-m\beta\phi(r)\right) + \frac{en_0}{\varepsilon\varepsilon_0}\exp\left(\beta\phi(r)\right), \tag{1}$$

where r is the distance from the slab center, e is the elementary charge, $\beta = e/k_bT$, $m = 1$ for single donors and 2 for double donors, $\varepsilon\varepsilon_0$ is the semiconductor permittivity, and N_{d0} and n_0 are the donor and electron concentrations in the center ($r = 0$) of the slab, determined by the following formulas:

$$N_{d0} = N_{ds}\exp\left(m\beta\phi_s\right), \tag{2}$$

$$n_0 = n_s\exp\left(-\beta\phi_s\right), \tag{3}$$

where N_{ds} and n_s are the donor and electron concentrations at the surface and ϕ_s is the surface potential.

The first and second boundary conditions are $\phi(r = 0) = 0$ and $d\phi/dr = 0$ in the slab center $r = 0$ [18]. The first term in (1) represents the contribution of the mobile donors at the temperature T, whereas the second term, including the charge distribution of electrons, was neglected because of the total depletion assumption [18].

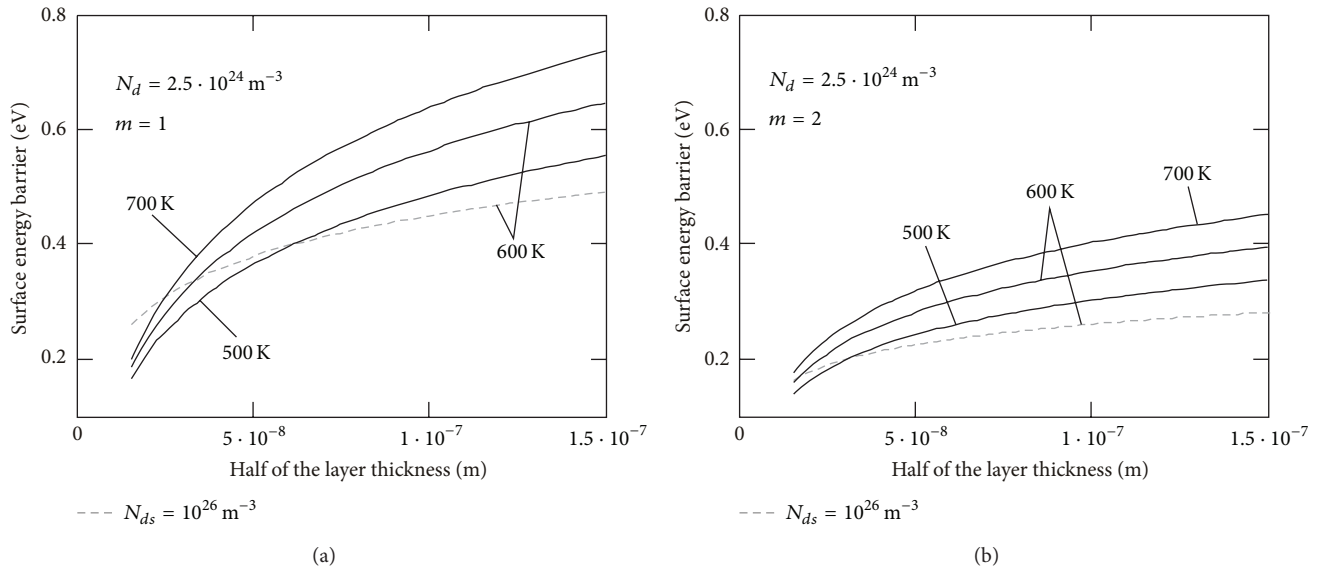

FIGURE 2: Full depletion layer. Surface energy barriers versus half of layer thickness, $N_d = 2.5 \times 10^{24}\ \mathrm{m}^{-3}$ for (a) single donors $m = 1$ and (b) double donors $m = 2$.

The analytical solution of (1) gives the following expression for the electric potential:

$$\phi(r) = -\frac{1}{m\beta} \ln\left(1 + tg^2\left(\frac{r}{\lambda}\right)\right), \tag{4}$$

and for the distribution of bulk donor concentration it gives

$$N_d(r) = N_{d0}\left(1 + tg^2\left(\frac{r}{\lambda}\right)\right), \tag{5}$$

where

$$\lambda^{-1} = \sqrt{\frac{em^2\beta N_{d0}}{2\varepsilon\varepsilon_0}}. \tag{6}$$

Assuming that donor concentration N_d is uniform in the bulk in no oxygen-containing atmosphere (before surface reaction with oxygen), we can write

$$\int_0^L N_d(r)\,dr = N_d L. \tag{7}$$

It should be noted that in our approach, the surface donor concentration N_{ds} was not a parameter, contrary to the assumption in [18].

The surface potential ϕ_s for different temperatures, layer thicknesses, and donor concentration N_d was obtained by solving the system of (2) and (4)–(7). The ϕ_s values were then applied as input data in the calculations of the surface total coverage with oxygen ions, coverage with various oxygen ions, and thus carrier concentration in-depth profile in the depletion layer [20]. These simulations were based on the solving of rate equations following [4]. In our approach based on the adsorption-desorption model proposed by Rantala et al. [4], all possible surface reactions and phenomena, that is, multistep oxygen adsorption, dissociation, recombination, and desorption, were taken into account. As a result of adsorption, the negative charge trapped in oxygen species causes an upward band bending and thus a reduced conductivity, when compared with that in the flat band condition. The data concerning the surface coverage by oxygen ions O_2^- and O^- needed for simulations were taken from [4, 21].

The sample conductance $G_\square$ was determined from the classical formula [9, 22] by using the obtained carrier concentration in-depth profiles:

$$G_\square = 2e\int_0^L \left(\mu_n n(x) + \mu_p p(x)\right)dx \approx 2e\int_0^L \left(\mu_n n(x)\right)dx, \tag{8}$$

where $n(x)$ and $p(x)$ are the electron and hole concentrations.

Because of the high doping of n-type SnO_2, the hole concentration in (8) was neglected. Furthermore, the gas pressure sensitivity α was calculated from the standard formulas. The calculations were carried out for n-SnO_2 layers with different thicknesses ($2 \times L$), from 30 nm to 500 nm, and doping level (single or double mobile bulk oxygen vacancies [23]) from $N_d = 1 \times 10^{24}\ \mathrm{m}^{-3}$ to $N_d = 2.5 \times 10^{25}\ \mathrm{m}^{-3}$ and within the temperature range from 300 K to 700 K. In the calculations, the carrier parameters, electron mobility $\mu_e = 150\ \mathrm{cm}^2/(\mathrm{Vs})$ at temperature 300 K and effective mass of electron equal to $0.3m_e$, were assumed. The temperature variations in the carrier mobility were taken from [24, 25].

3. Results and Discussion

An influence of temperature (from 400 K to 700 K) and doping on the surface energy barrier are shown in Figure 1(b). From Figure 1(b), it is evident that the surface band bending between 0.16 eV and 0.41 eV (at 600 K) can be obtained

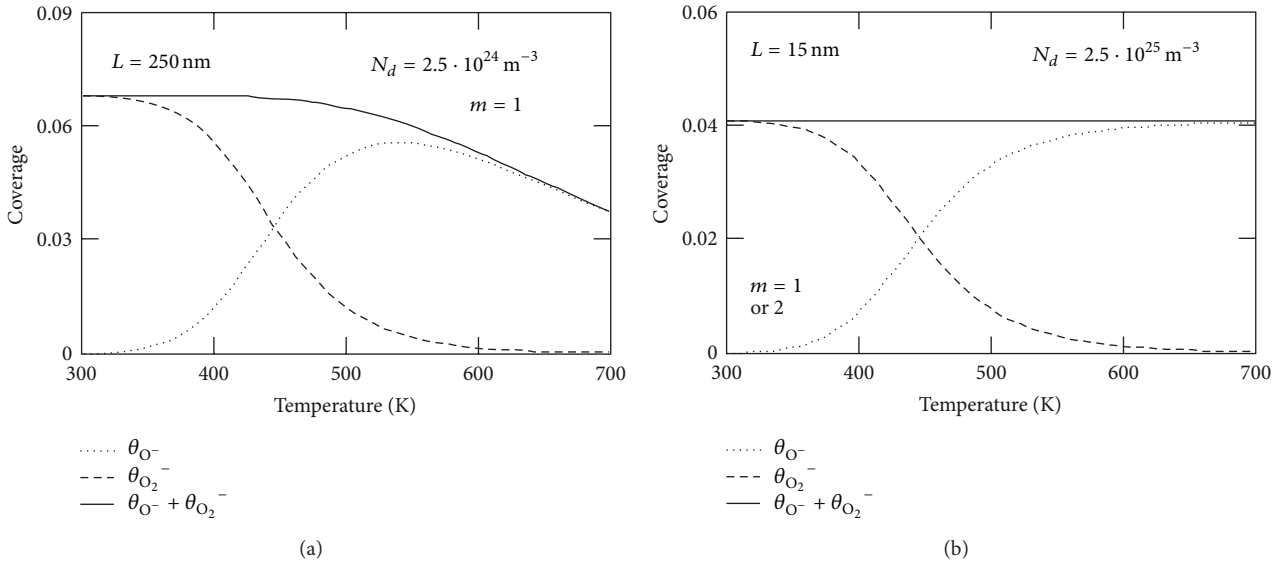

FIGURE 3: Calculated coverage of the oxygen ions O^- and $O_2{}^-$ and total coverage ($O^- + O_2{}^-$) versus temperature in dry synthetic air, for mobile (a) single-donor concentration, $N_d = 2.5 \times 10^{24}$ m^{-3} and $L = 250$ nm, and (b) single- and double-donor concentrations, $N_d = 2.5 \times 10^{25}$ m^{-3}, and $L = 15$ nm.

for a relatively high donor concentration (2.5×10^{24}–2.5×10^{25} m^{-3}), if the thickness of the SnO_2 plate is $2 \times L = 30$ nm. On the other hand, in the presence of oxygen, in temperatures ranging from 400 K to 700 K, the band bending increases from 0.24 eV to 0.35 eV (for single-ionized oxygen vacancies: $m = 1$) and from 0.17 eV to 0.26 eV (for double-ionized oxygen vacancies: $m = 2$), if donor concentration is $N_d = 1 \times 10^{25}$ m^{-3} and $2 \times L = 30$ nm (Figure 1(b)). The surface barrier grows along with the rise in donor concentration N_d throughout the investigated temperature range for various thicknesses of the layer.

The calculated energy barrier values are in line with the results obtained by Rantala and Lantto [18]. The height of the barrier is influenced both by the thickness and the degree of donor ionization (Figure 2). For example, at 700 K, a change in the thickness of the layer from 15 nm to 150 nm is accompanied by an increase in eVs from 0.20 eV to approximately 0.74 eV, when $m = 1$ (Figure 2(a)), or an increase from 0.18 eV to 0.45 eV, when $m = 2$ (Figure 2(b)). The energy barrier for double-ionized donors is lower than that in the case of single-ionized donors (at the same temperature, for equal N_d concentrations, and the same layer thickness). The results of the calculations were compared with the ones obtained by Rantala and Lantto [18], who assumed a constant value of donor concentration near the surface $N_{ds} = 10^{26}$ m^{-3}. Differences between the respective curves (Figure 2, $T = 600$ K) result from different beginning conditions in calculations, namely, each continuous curve point in Figure 2 corresponds to the same value of donor concentration N_d (uniform in the bulk before surface reaction with oxygen); however, every point of the intermittent curve corresponds to different donor concentration values N_d in a sample of a given thickness.

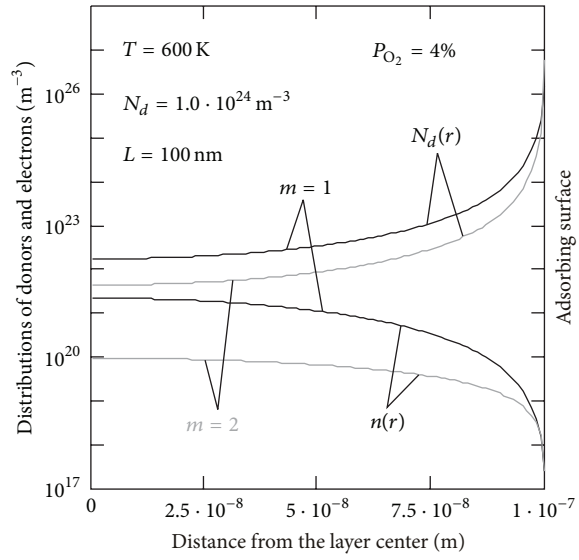

FIGURE 4: In-depth profiles of mobile donor $N_d(r)$ and electron $n(r)$ concentrations for single ($m = 1$) and double ($m = 2$) donors at temperature $T = 600$ K, $N_d = 10^{24}$ m^{-3}, and $L = 100$ nm.

The calculated total coverage by oxygen species and the coverages of the oxygen ions O^- and $O_2{}^-$ versus temperature in dry synthetic air, for mobile single donors ($N_d = 2.5 \times 10^{24}$ m^{-3}, $L = 250$ nm) and for mobile double donors ($N_d = 2.5 \times 10^{25}$ m^{-3}, $L = 15$ nm), are shown in Figure 3. The calculations suggest that the coverages of the atomic and molecular ionic species are equal at a temperature of about 445 K. The calculated temperature corresponds to the transition temperature of 423 K, found by Chang [8, 26], as a

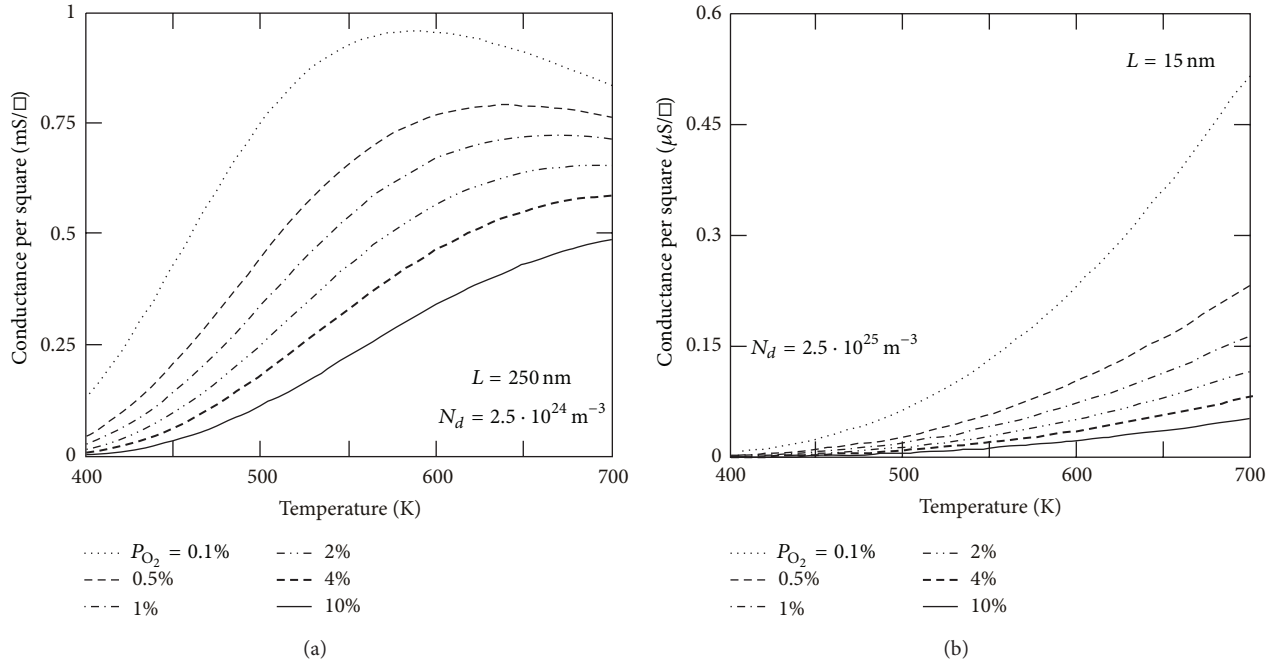

FIGURE 5: Per-square conductance versus temperature for (a) $N_d = 2.5 \times 10^{24}\ \mathrm{m}^{-3}$, $L = 250\ \mathrm{nm}$, and $m = 1$ and (b) $N_d = 2.5 \times 10^{25}\ \mathrm{m}^{-3}$, $L = 15\ \mathrm{nm}$, and $m = 1$, for different oxygen partial pressures P_{O_2}.

result of measurements of ~100 nm thick SnO_2 nanolayers, deposed on Al_2O_3 using a method of reactive deposition from the target containing powdered tin dioxide. Compatible experimental results were reported by Rembeza et al. [27] while investigating nanocrystalline layers with grain diameter < 20 nm (layer thickness > 1 μm) formed by means of magnetron cathode deposition on glass substrates. The dynamics of the changes of total coverage by oxygen ions depends on grain thickness and the degree to which the donors are ionized and, in the case of very thin layers, is negligible (see Figure 3(b)). Total coverage by oxygen ions is strongly dependent on temperature and donor concentration (Figure 3(a)) if the thickness of a totally depleted layer is relatively high ($L > 150$ nm).

Figure 4 shows the charge distribution in the case of mobile single and double donors at temperature $T = 600$ K if the content of oxygen in nitrogen is $P = 4\%$, and half of the layer thickness $L = 100$ nm. From the calculations, it is observed that SnO_2 thin films may be depleted from electrons in the atmospheric air in the case of mobile donors.

The surface space charge region, induced by adsorbed ions, contributes significantly to the conductance of the semiconducting SnO_2 layers. The sample per-square conductance was determined from the classical formula [9, 22], using the obtained in-depth carrier profiles (Figure 4). The dependence of the per-square conductance on temperature for different partial pressures of oxygen and slab thicknesses is shown in Figure 5. The calculations show that the maximum per-square conductance shifts in the direction of lower temperatures if the partial pressure of oxygen decreases or when N_d increases (Figure 5(a)). Experimentally, the maximum conductance was observed at 450 K for nanocrystalline layers of SnO_2 with grain diameter < 20 nm and between 550 K and 600 K for polycrystalline, thin layers less than 500 nm and average grain size 15 nm [28]. The results of conductivity measurements of SnO_2 layers may vary considerably; they depend on the surface structure (its stoichiometry and defectiveness), the layer smoothness, the type of the substrate, and the different methods of layer forming. For the slabs with dimensions smaller than the space charge region and relatively low oxygen concentration, a strong change in the conductance is observed (Figure 5(b)). If the thickness of SnO_2 sample decreases, the ratio of the thickness of depletion layer and thickness of the sample increases; the sample of SnO_2 thin layer can be depleted as a whole and the conductance of the sample is small [22, 29].

From Figure 6(a), it is evident that the per-square conductance depends on the layer thickness. The calculations show that the maximum per-square conductance shifts in the direction of lower temperatures if the thickness of the slab increases. Experimentally, within the temperature range between about 420 K and 723 K, the maximum conductance was observed at temperature above 600 K in the case of thin films [28, 30, 31] and at lower temperatures (555 K) in the case of thick films [30–32]. The sensitivity with respect to the partial pressure of oxygen (power coefficient α) versus temperature is independent of the degree of donor ionization for the slab thickness ($2 \times L$) lower than 150 nm, as it is observed in Figure 6(b). The value of the coefficient α changes in the range from −0.55 ($L < 70$ nm) to −0.34 ($L = 200$ nm) for the sensor working temperature between 500 K and 700 K.

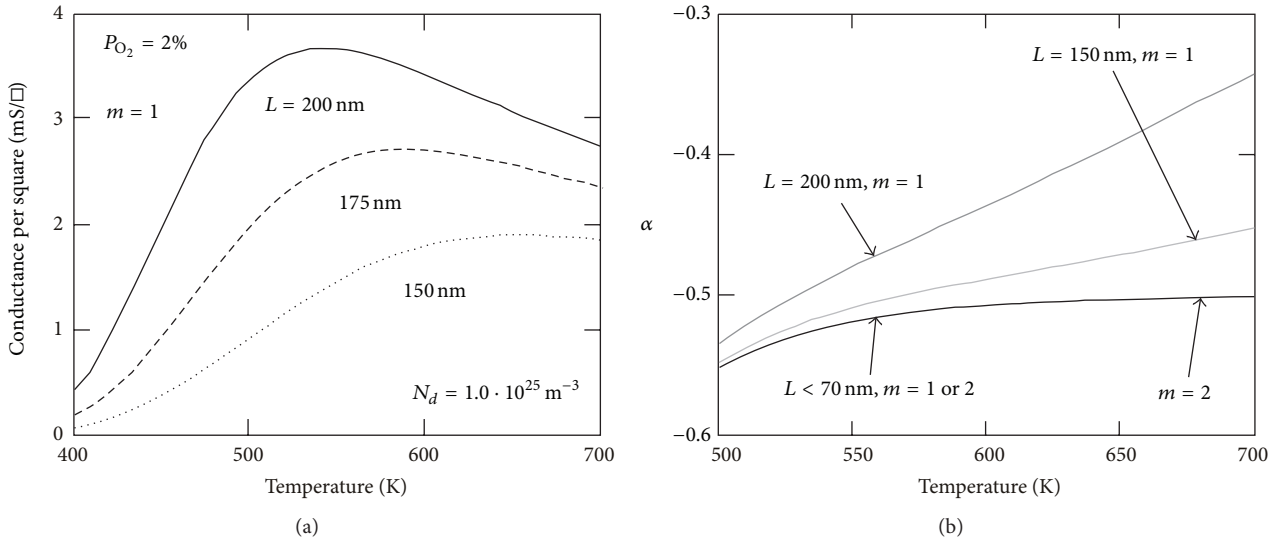

FIGURE 6: (a) Per-square conductance versus temperature for different half of the layer thickness. (b) Sensitivity with respect to partial pressure of oxygen in ambient atmosphere (power coefficient α) versus temperature, $N_d = 2.5 \times 10^{24}$ m^{-3}, for different half of the layer thickness.

This result is consistent with [33], where the calculations performed on the basis of acting mass low give $\alpha = -0.5$ for the constant concentration of oxygen lattice defects (oxygen vacancies). Experimentally, the values of α were between -0.25 and -0.5 [11]. For thick, porous layers of SnO_2, $\alpha = -0.38$ was obtained [11]; in the case of thin, polycrystalline layers, for which the changed grain size was ranging from 100 nm to 500 nm, α coefficient value was -0.5 [10].

4. Summary and Conclusions

A numerical analysis of oxygen adsorption on the surface of flat-geometry grains was carried out. It was proved that the depth profiles of potential and the value of surface energy barrier are strongly influenced by the temperature, the layer thickness, and the degree of donor ionization. With the use of computer simulations, it was reported that the coverage by ionized oxygen species (O_2^- and O^-) and layer conductivity strongly depend on its thickness (from 30 nm to 500 nm).

It was demonstrated that the presence of oxygen in ambient air leads to a decrease in the conductivity of the nanolayer as the partial pressure of oxygen increases. In a range of temperatures, from 500 K to 700 K, the found α index values (sensitivity in relation to oxygen partial pressure) are in conformity with the theoretical and experimental data obtained as a result of the interaction of the surface with oxygen. Theoretical analysis of oxygen adsorption on the surface of SnO_2, in a single-dimension case for flat-geometry grains (the so-called *slab model*), is an accurate approximation of electron properties of surface and near-surface region of thin epitaxial layers and small grains (SnO_2 layer based sensors), for which the thickness of the depleted layer is comparable with the grain radius.

Conflict of Interests

The author declares that there is no conflict of interests regarding the publication of this paper.

References

[1] J. C. M. Brokken-Zijp, O. L. J. van Asselen, W. E. Kleinjan, R. van de Belt, and G. de With, "Photocatalytic properties of tin oxide and antimony-doped tin oxide nanoparticles," *Journal of Nanotechnology*, vol. 2011, Article ID 106254, 15 pages, 2011.

[2] F. Flitti, A. Far, B. Guo, and A. Bermak, "A robust and low-complexity gas recognition technique for on-chip tin-oxide gas sensor array," *Journal of Sensors*, vol. 2008, Article ID 465209, 6 pages, 2008.

[3] G. Lu, K. L. Huebner, L. E. Ocola, M. Gajdardziska-Josifovska, and J. Chen, "Gas sensors based on tin oxide nanoparticles synthesized from a mini-arc plasma source," *Journal of Nanomaterials*, vol. 2006, Article ID 60828, 7 pages, 2006.

[4] T. S. Rantala, V. Lantto, and T. T. Rantala, "Rate equation simulation of the height of Schottky barriers at the surface of oxidic semiconductors," *Sensors and Actuators B*, vol. 13, no. 1–3, pp. 234–237, 1993.

[5] W. Izydorczyk, B. Adamowicz, M. Miczek, and K. Waczynski, "Computer analysis of an influence of oxygen vacancies on the electronic properties of the SnO_2 surface and near-surface region," *Physica Status Solidi (A)*, vol. 203, no. 9, pp. 2241–2246, 2006.

[6] J. Pan, H. Shen, and S. Mathur, "One-dimensional SnO_2 nanostructures: synthesis and applications," *Journal of Nanotechnology*, vol. 2012, Article ID 917320, 12 pages, 2012.

[7] M. Habgood and N. Harrison, "An ab initio study of oxygen adsorption on tin dioxide," *Surface Science*, vol. 602, no. 5, pp. 1072–1079, 2008.

[8] S. C. Chang, "Sensing mechanisms of thin-film tin oxide," in *Proceedings of the International Meeting on Chemical Sensors*, pp. 78–83, Fukuoka, Japan, September 1983.

[9] S. R. Morrison, *The Chemical Physics of Surfaces*, Plenum Press, New York, NY, USA, 1997.

[10] V. V. Kissine, V. V. Sysoev, and S. A. Voroshilov, "Conductivity of SnO_2 thin films in the presence of surface adsorbed species," *Sensors and Actuators B*, vol. 79, no. 2-3, pp. 163–170, 2001.

[11] V. Lantto, P. Romppainen, and S. Leppävuori, "Response studies of some semiconductor gas sensors under different experimental conditions," *Sensors and Actuators*, vol. 15, no. 4, pp. 347–357, 1988.

[12] K. D. Schierbaum, H. D. Wiemhöfer, and W. Göpel, "Defect structure and sensing mechanism of SnO_2 gas sensors: comparative electrical and spectroscopic studies," *Solid State Ionics*, vol. 28–30, part 2, pp. 1631–1636, 1988.

[13] J. Mizsei and V. Lantto, "Simultaneous response of work function and resistivity of some SnO_2-based samples to H_2 and H_2S," *Sensors and Actuators B*, vol. 4, no. 1-2, pp. 163–168, 1991.

[14] S. Semancik and D. F. Cox, "Fundamental characterization of clean and gas-dosed tin oxide," *Sensors and Actuators*, vol. 12, no. 2, pp. 101–106, 1987.

[15] T. G. G. Maffes, G. T. Owen, M. W. Penny et al., "Nanocrystalline SnO_2 gas sensor response to O_2 and CH_4 at elevated temperature investigated by XPS," *Surface Science*, vol. 520, no. 1-2, pp. 29–34, 2002.

[16] B. Slater, C. R. A. Catlow, D. E. Williams, and A. M. Stoneham, "Dissociation of O_2 on the reduced SnO_2 (110) surface," *Chemical Communications*, no. 14, pp. 1235–1236, 2000.

[17] J. Oviedo and M. J. Gillan, "First-principles study of the interaction of oxygen with the SnO_2 (110) surface," *Surface Science*, vol. 490, no. 3, pp. 221–236, 2001.

[18] T. S. Rantala and V. Lantto, "Some effects of mobile donors on electron trapping at semiconductor surfaces," *Surface Science*, vol. 352–354, pp. 765–770, 1996.

[19] U. Pulkkinen, T. T. Rantala, T. S. Rantala, and V. Lantto, "Kinetic Monte Carlo simulation of oxygen exchange of SnO_2 surface," *Journal of Molecular Catalysis A*, vol. 166, no. 1, pp. 15–21, 2001.

[20] W. Izydorczyk and B. Adamowicz, "Computer analysis of oxygen adsorption at SnO_2 thin films," *Optica Applicata*, vol. 37, no. 4, pp. 377–386, 2007.

[21] S. R. Morrison, "Mechanism of semiconductor gas sensor operation," *Sensors and Actuators*, vol. 11, no. 3, pp. 283–287, 1987.

[22] N. Barsan and U. Weimar, "Conduction model of metal oxide gas sensors," *Journal of Electroceramics*, vol. 7, no. 3, pp. 143–167, 2001.

[23] N. Murakami, K. Tanaka, K. Sasaki, and K. Ihokura, "Influence of sintering temperature on characteristics of tin oxide combustion monitor sensors," in *Proceedings of the International Meeting on Chemical Sensors*, pp. 165–170, Fukuoka, Japan, September 1983.

[24] R. Summitt and N. F. Borrelli, "Temperature dependence of the ultraviolet absorption edges in SnO_2," *Journal of Applied Physics*, vol. 37, no. 5, p. 2200, 1966.

[25] C. G. Fonstad and R. H. Rediker, "Electrical properties of high-quality stannic oxide crystals," *Journal of Applied Physics*, vol. 42, no. 7, pp. 2911–2918, 1971.

[26] S. C. Chang, "Oxygen chemisorption on tin oxide: correlation between electrical conductivity and EPR measurements," *Journal of Vacuum Science & Technology*, vol. 17, no. 1, pp. 366–369, 1980.

[27] S. I. Rembeza, E. S. Rembeza, T. V. Svistova, and O. I. Borsiakova, "Electrical resistivity and gas response mechanisms of nanocrystalline SnO_2 films in a wide temperature range," *Physica Status Solidi (A)*, vol. 179, no. 1, pp. 147–152, 2000.

[28] R. Sanjines, F. Lévy, V. Demarne, and A. Grisel, "Some aspects of the interaction of oxygen with polycrystalline SnO_x thin films," *Sensors and Actuators B*, vol. 1, no. 1–6, pp. 176–182, 1990.

[29] F. Cosandey, G. Skandan, and A. Singhal, "Materials and processing issues in nanostructured semiconductor gas sensors," *JOM-e*, vol. 52, no. 10, pp. 1–6, 2000.

[30] B. Adamowicz, W. Izydorczyk, J. Izydorczyk, A. Klimasek, W. Jakubik, and J. Zywicki, "Response to oxygen and chemical properties of SnO_2 thin-film gas sensors," *Vacuum*, vol. 82, no. 10, pp. 966–970, 2008.

[31] Th. Becker, S. Ahlers, Ch. B.-V. Braunmuhl, G. Müller, and O. Kiesewetter, "Gas sensing properties of thin- and thick-film tin-oxide materials," *Sensors and Actuators B*, vol. 77, no. 1-2, pp. 55–61, 2001.

[32] V. Lantto and V. Golovanov, "A comparison of conductance behaviour between SnO_2 and CdS gas-sensitive films," *Sensors and Actuators B*, vol. 25, no. 1–3, pp. 614–618, 1995.

[33] L. Yu. Kupriyanow, *Semiconductor Sensors in Physico-Chemical Studies*, Elsevier, Amsterdam, The Netherlands, 1996.